Functional Nuclear Organization of Transcription and DNA Replication

A Topographical Marriage between Chromatin Domains and the Interchromatin Compartment

Y. Markaki,[1] M. Gunkel,[2] L. Schermelleh,[3] S. Beichmanis,[2] J. Neumann,[3] M. Heidemann,[4] H. Leonhardt,[3,5] D. Eick,[4,5] C. Cremer,[2] and T. Cremer[1,5]

[1]LMU Biocenter, Department of Biology II, Anthropology and Human Genetics, Ludwig Maximilians University (LMU), Martinsried D-82152, Germany; [2]University Heidelberg, Kirchhoff-Institute for Physics and BioQuant Center, Heidelberg D-69120, Germany; [3]LMU Biocenter, Department of Biology II, Epigenetics, Ludwig Maximilian University of Munich (LMU), Martinsried D-82152, Germany; [4]Helmholtz Center Munich, Department of Molecular Epigenetics, Munich D-81377, Germany; [5]Center for Integrated Protein Science, Martinsried D-82152, Germany

Correspondence: Thomas.Cremer@lrz.uni-muenchen.de

We studied the nuclear topography of RNA transcription and DNA replication in mammalian cell types with super-resolution fluorescence microscopy, which offers a resolution beyond the classical Abbe/Raleigh limit. Three-dimensional structured illumination microscopy (3D-SIM) demonstrated a network of channels and wider lacunas, called the interchromatin compartment (IC). The IC starts at nuclear pores and expands throughout the nuclear space. It is demarcated from the compact interior of higher-order chromatin domains (CDs) by a 100–200-nm thick layer of decondensed chromatin, termed the perichromatin region (PR). Nascent DNA, nascent RNA, RNA polymerase II (RNA Pol II), as well as histone modifications for transcriptionally competent/active chromatin, are highly enriched in the PR, whereas splicing speckles are observed in the interior of the IC. In line with previous electron microscopic evidence, spectral precision distance/position determination microscopy (SPDM) confirmed the presence of RNA Pol II clusters indicative of transcription factories. Still, a substantial part of transcription apparently takes place outside of such factories. Previous electron microscopic evidence has suggested that the functional nuclear organization of DNA replication depends on Brownian movements of chromatin between the CD interior and the PR. As an incentive for future studies, we hypothesize that such movements also take place during transcription, i.e., only the actually transcribed part of a gene may be located within the PR, whereas its major part, including previously or later transcribed sequences, is embedded in a higher-order chromatin configuration in the interior of the CD.

Current models of nuclear architecture concur that nuclei of multicellular organisms contain chromosome territories (CTs) (Cremer and Cremer 2010). It is now generally accepted that nuclear arrangements of CTs, as well as chromatin order within CTs, are nonrandom and can undergo major changes during cell differentiation and upon certain functional demands (Solovei et al. 2009; Mehta et al. 2010; Schoenfelder et al. 2010). Chromatin domains (CDs) with a DNA content of a few hundred kilobases to several megabases (~1-Mb CDs) have been described as basic structural features of CTs (Ma et al. 1998; Cremer and Cremer 2001). Each ~1-Mb CD persists throughout interphase and acts as a replication focus at a given time during S phase (Sparvoli et al. 1994; Jackson and Pombo 1998; Zink et al. 1999; Berezney et al. 2000). In turn, ~1-Mb CDs are likely built up from multiple chromatin loops with a DNA content of some 50 to 200 kb (Münkel et al. 1999; Li et al. 2006). However, structural details of CDs and implications of dynamic interactions in *cis* (within the same CT) and in *trans* (between different CTs) on major nuclear functions, such as transcription, splicing, and DNA replication and repair, are still not well understood (Rouquette et al. 2010).

Conventional confocal images revealed a diameter of ~500 nm for replication foci (Albiez et al. 2006), whereas diameters ranging between 40 and 210 nm were detected at higher resolution (Koberna et al. 2005; Baddeley et al. 2009), indicating that conventional light optical measurements were erroneous because of the limited resolution. Arguably, CDs are built up from a hierarchy of chromatin fibers and loops ranging from 10-nm- and 30-nm-thick fibers to even higher levels of chromatin compaction. CTs and ~1-Mb CDs are interconnected by chromatin fibers and apparently constitute a global higher-order three-dimensional (3D) chromatin network (Albiez et al. 2006).

Evidence obtained by cryo-electron microscopy (cryo-EM) has shown that clumps of condensed chromatin are composed of finely granular, rather homogeneous material and called into question the presence of 30-nm-thick chromatin fibers in mitotic chromosomes (Maeshima and Eltsov 2008; Maeshima et al. 2010) or CTs (Bouchet-Marquis et al. 2006; Eltsov et al. 2008). Arguably, nucleosome fibers in vivo form an interdigitated state like a "polymer melt" (Maeshima et al. 2010). The "polymer melt" concept implies highly dynamic polymer chains constantly moving and rearranging at the local level (de Gennes 1979). Maeshima et

al. (2010) argued that selective intrafiber nucleosomal associations, necessary for the formation of 30-nm-thick chromatin fibers, require dilute conditions present only in in vitro systems. At high nucleosome concentrations that occur in vivo, interfiber nucleosome interactions become increasingly dominant, and nucleosome fibers are forced to interdigitate with one another to an extent that "the nucleosome does not 'know' to which fiber it belongs." Accordingly, these investigators have compared CDs with drops of viscous liquid formed by nucleosome–nucleosome interactions and macromolecular crowding effects. Although they consider the "polymer melt" as a highly disordered state, this model does not exclude a highly dynamic, functionally important organization of such chromatin droplets. In line with the perichromatin region (PR) concept (Fakan and van Driel 2007) and our present observations, the "chromatin liquid drop" model predicts that transcription is inhibited inside of the chromatin liquid drops and only allowed on the drop surfaces.

INTERCHROMATIN COMPARTMENT AND PERICHROMATIN REGION

The chromosome territory–interchromatin compartment (CT-IC) model argues for an interconnected network of apparently DNA-free channels and lacunas, termed the interchromatin compartment (IC), expanding in between this global chromatin network (Cremer et al. 2000; Cremer and Cremer 2001, 2010). The IC channels emanate at nuclear pores and expand both at the periphery of CTs and into their interior. The interior of wider IC lacunas (≥400 nm) is apparently DNA-free and contains nuclear bodies and splicing speckles (Albiez et al. 2006). The width of IC channels is highly variable and likely influenced by Brownian movements of CDs. This dynamic behavior allows transient contacts of domain surfaces in *cis* and in *trans* and thus provides opportunities for chromosomal rearrangements (Kreth et al. 2004a,b, 2007), as well as the formation of nonrandom chromatin interactions, which may be stabilized after a random contact (Lieberman-Aiden et al. 2009; Schoenfelder et al. 2010). Furthermore, the CT-IC model takes into account that the supposedly more compact interior of CDs is separated from the IC by a roughly 100–200-nm-thick layer of decondensed chromatin, called the perichromatin region (PR) (Fakan and Hancock 1974; Fakan and van Driel 2007; Niedojadlo et al. 2011). The PR is considered as the nuclear subcompartment where transcription, cotranscriptional splicing, DNA replication, and possibly also DNA repair take place. During ongoing transcription chromatin representing single transcribed genes may be entirely located in a decondensed form within the PR. Alternatively, it seems possible that only the actually transcribed part of a gene is located within the PR, whereas chromatin carrying previously or later transcribed sequences is embedded in a higher-order compaction in the interior of the CD.

Transcription occurs either in perichromatin fibrils (PFs) located in the PR, or in transcription factories (TFs). PFs represent the in situ form of individual nucleoplasmic RNA transcripts and also the site where cotranscriptional splicing occurs (Monneron and Bernhard 1969; Fakan 2004; Fakan and van Driel 2007). Available data suggest that transcription and, accordingly, most active RNA Pol II, might be restricted to TFs (Cook 2010). The structure and composition of TFs are far from being clear. They could serve as platforms for efficient gene transcription of any gene placed in the next neighborhood of any given factory. Alternatively, specialized TFs have been reported, where specific genes can be transcribed in a coregulated manner (Osborne et al. 2007; Schoenfelder et al. 2010). Whether the initiation of transcription of individual genes occurs before or after their association with such a factory is unknown. It has been shown that TFs persist in the absence of transcription (Palstra et al. 2008), and possibly a TF is not involved in the start of the transcription, but in its enhancement.

Splicing speckles located in the IC supply splicing factors to PFs and TFs, whereas chromatin fibers spare mainly, or even entirely, the interior of the IC, in particular, the interior of wider IC lacunas (Albiez et al. 2006). The IC may be compared with a meandering river featuring many side arms, whereas the PR reflects its natural embankment. The PR has a highly nonrandom topography, yet, in contrast to an artificially designed embankment, its configuration also has a stochastic component. The natural embankment, for example, is not uniformly delimited from the riverbed like a man-made concrete wall, but rather extends more or less freely into the riverbed. Notably, IC channels start at nuclear pores and penetrate through the underlying lamina (Schermelleh et al. 2008). However, to which extent the PR or the IC or both may serve as preferential nuclear compartments for the export of spliced RNA to the nuclear pores is not known. Macromolecules apparently can invade compact chromatin (Gorisch et al. 2003, 2005). Thus it can be argued that RNPs on their way to nuclear pores may penetrate barriers of chromatin. Further studies are necessary to learn more about the penetration of macromolecules and macromolecule complexes with different sizes and electric charges into and through compact chromatin (Finan and Guilak 2010; Grünwald and Singer 2010).

The existence of both the IC and the PR as structurally and functionally distinct nuclear subcompartments has been disputed (Branco and Pombo 2006). Many schematic representations of nuclear architecture in publications and textbooks still depict chromatin organization as 3D networks of fibers. Although an interchromatin space exists between such chromatin fiber networks, the respective models suggest that transcription and other nuclear functions can be carried out along decondensed 10- or 30-nm-thick chromatin fibers (for review, see Rouquette et al. 2010).

MICROSCOPIC METHODS USED IN THE PRESENT STUDY: 3D-SIM AND SPDM

The diverse states of higher-order chromatin organization in different cell types show the demand for identifying distinct cell-type/phase-specific features of single fixed and living cells. Recently, the resolution limit of classical light microscopy has been overcome by super-resolution microscopy methods (for reviews, see Hell 2009; Huang et al. 2009; Cremer et al. 2010; Rouquette

et al. 2010; Schermelleh et al. 2010). For a high-resolution examination of the nuclear topography of DNA, nascent RNA, and nascent DNA, as well as RNA Pol II and histone modifications H3K4me3 and H4K8ac, typical for transcriptionally competent chromatin, we used two types of light optical nanoscopy: three-dimensional structured illumination microscopy (3D-SIM) (Gustaffson et al. 2008; Schermelleh et al. 2008) and spectral precision distance/position determination microscopy (SPDM) (Cremer et al. 1999, 2010; Gunkel et al. 2009; Lemmer et al. 2009; Bohn et al. 2010). In SIM a fluorescent specimen is illuminated with a series of sinusoidal striped patterns of high spatial frequency generated by laser light passing through a movable optical grating (Heintzmann and Cremer 1999; Gustafsson 2000). The procedure yields coarser, bar code–like interference patterns—moiré fringes—in the microscope's image plane, which are recorded in different orientations. Processing of all acquired images by dedicated computer algorithms yields a high-resolution image of the underlying fine structure with a lateral resolution increased by a factor of 2 beyond the classical diffraction limit. With 3D-SIM an additional twofold increase in the axial resolution can be achieved (Gustafsson et al. 2008; Schermelleh et al. 2008). 3D-SIM allows multispectral optical sectioning with a lateral (x, y) resolution of 100–130 nm and an axial (x, z) resolution of 250–300 nm. Thus, compared to conventional confocal laser scanning microscopy, 3D-SIM detects ensembles of emitting fluorophores with an approximately eightfold improved resolved volume (Schermelleh et al. 2010). SPDM, in contrast, allows time-resolved single-molecule localization depending on the sequential imaging of bursts of photons emitted from individual "blinking" fluorophores with a localization accuracy of a few nanometers in the lateral plane of the specimen. Notably, the serial recording of blinking fluorophores allows the individual detection of two fluorophores, which even have nearly the same spatial coordinates. Two blinking fluorophores, which emit at different times, can be resolved down to a distance of ~10 nm. SPDM microscopy is presently the most rapid procedure of spectrally assigned localization microscopy (SALM). Importantly, blinking can be induced in conventional fluorophores, such as GFP and Alexa dyes, using light at a given wavelength and a critical illumination intensity in the object plane. In contrast, related SALM techniques, such as photoactivated localization microscopy (PALM) (Betzig et al. 2006) and stochastic optical reconstruction microscopy (STORM) (Rust et al. 2006), require a much more time-consuming illumination of special, photoswitchable fluorophores at two different wavelengths (for reviews, see Cremer et al. 2010; Patterson et al. 2010).

In our present study, we used both 3D-SIM and SPDM. 3D-SIM was performed on a DeltaVision OMX V3 prototype (Applied Precision). For SPDM, we used a prototype built in the C. Cremer laboratory at the University of Heidelberg (Reymann et al. 2008; Gunkel et al. 2009). Indirect immunofluorescence was performed with primary antibodies carefully tested for their specificity (Kontermann et al. 1995; Chapman et al. 2007).

TOPOGRAPHY OF NUCLEAR DNA STUDIED WITH 3D-SIM

C127 cells were derived from a mouse mammary tumor (Lowy et al. 1978) and possess a quite large and flat nucleus. Figure 1 shows light optical (x, y) and (z, x) sections through a DAPI (4′,6-diamidino-2-phenylindole dihydrochloride)–stained nucleus obtained by 3D-SIM, as well as a part of a 3D nuclear reconstruction. In line with a previous 3D electron microscopic study (Rouquette et al. 2009), the nucleus shows brightly stained chromocenters, typically associated with the nuclear lamina or the perinucleolar compartment (Németh et al. 2010). Furthermore, interconnected assemblies of CDs are visualized, in line with EM/ESI data from Bazett-Jones and coworkers (Ahmed et al. 2010). However, in the absence of a dedicated labeling protocol, e.g., by a BrdU pulse, it is not possible to unequivocally discriminate individual CDs. The resolution limit of 3D-SIM does not allow a more detailed analysis of the possible contribution of 10-nm- and 30-nm-thick chromatin fibers, or even 60–80-nm-thick chromonema fibers. 3D-SIM, however, clearly delineates the presence of an IC expanding between the 3D chromatin network. Its width ranges from wide lacunas (diameters ≥400 nm) to narrow channels. The smallest channels may provide access to the interior of ~1-Mb chromatin domains. Because DAPI stains preferentially AT-rich DNA, it does not exclude the possibility that GC-rich DNA is present in the interior of wider IC channels and lacunas. Unfortunately, current limitations precluded the use of other DNA dyes useful for staining GC-rich DNA. The sparsity, if not absence, of chromatin loops or naked DNA in the interior of wider channels and IC lacunas is supported by two additional findings: (1) a 3D electron microscopic study using a highly selective and sensitive protocol for DNA staining at the ultrastructural level (Rouquette et al. 2009) and (2) the probing of histone modifications representative of transcriptionally competent chromatin (see below).

NUCLEAR TOPOGRAPHY OF RNA POL II STUDIED WITH 3D-SIM

RNA Pol II together with numerous other proteins forms the machinery for the synthesis of mRNA precursors, most snRNAs and microRNAs. RNA Pol II consists of two major subunits, RPB1 and RPB2 and 10 smaller subunits (Jackson et al. 1998; Kimura et al. 2002). The carboxy-terminal domain (CTD) of its RPB1 subunit comprises multiple heptapeptide repeats (52 in mammalian cells) of the consensus sequence Y-S-P-T-S-P-S. The CTD domain is subject to posttranslational modifications, including phosphorylation of serine 2 and serine 5. Different phosphorylation states or levels reflect stages and events of the transcription cycle. For instance, the initiating form of RNA Pol II is phosphorylated at serine 5 (Ser5P) and bound onto promoter sites of genes, whereas the elongating (active) form is more heavily phosphorylated at serine 2 (Ser2P). At the end of transcription, the phosphorylation of serine 5 is removed by CTD phosphatases, whereas Ser2P-RNA Pol II accumulates at

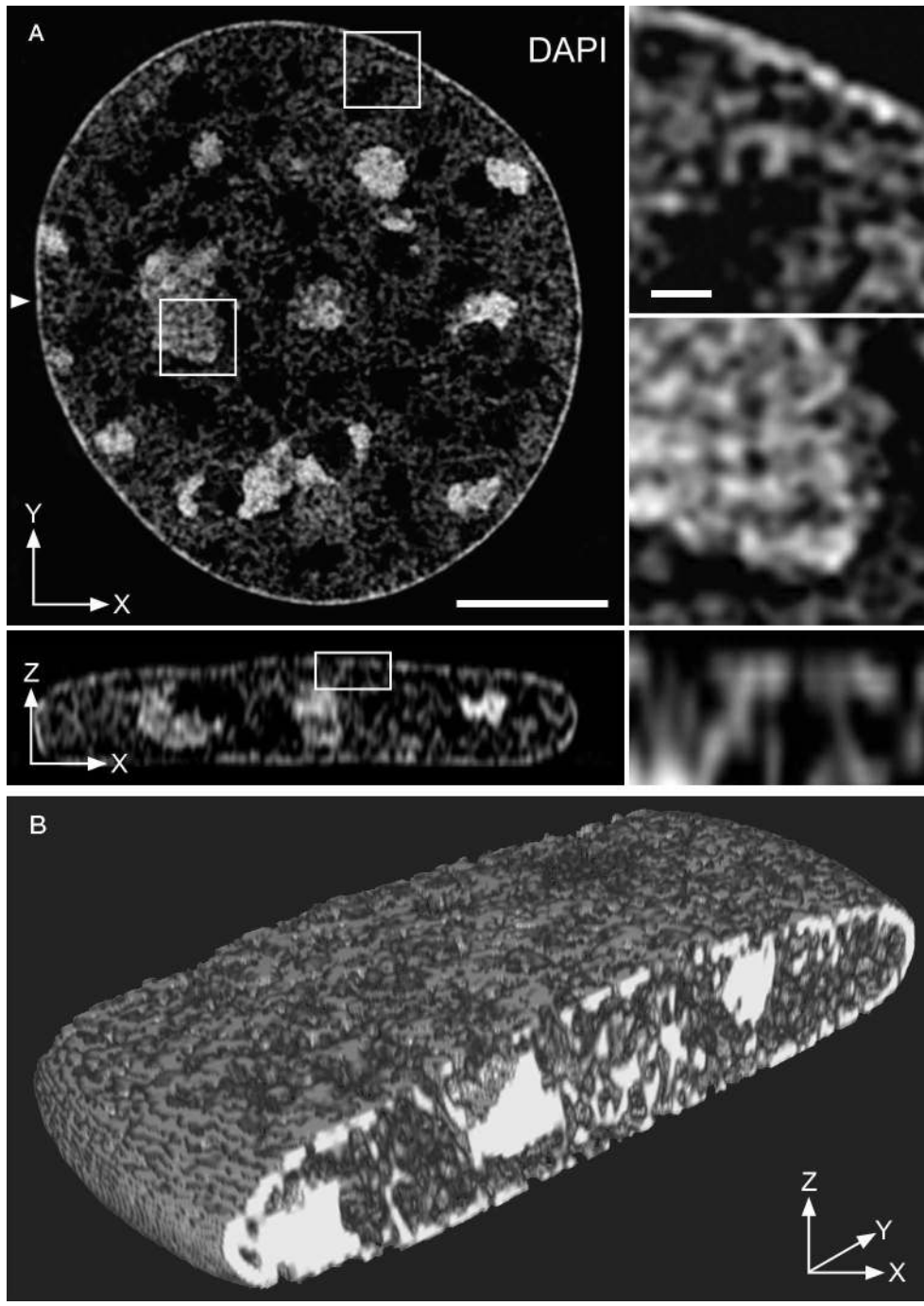

Figure 1. Nuclear topography of DAPI-stained DNA. (*A*, *left* side) Lateral (*x*, *y*) (*top*) and orthogonal (*x*, *z*) (*bottom*) optical cross-sections through a DAPI-stained C127 cell nucleus recorded with 3D-SIM. Bar, 5 µm. (*Right* side) 4× Magnification of marked regions shown in the *left* images. Bar, 500 nm. (*B*) Part of a 3D reconstruction of the nucleus in *A*. Note the lack of DAPI-stained DNA in the interior of IC lacunas. This lack is in line with previous 3D-EM studies demonstrating that the interiors of IC lacunas are not invaded by DNA loops (Rouquette et al. 2009).

the 3′ end of the gene (Egloff and Murphy 2008). To study the nuclear topography of RNA Pol II in mouse C127 cells, we made use of three monoclonal antibodies: Mouse monoclonal antibody Pol 3/3, originally raised against the *Drosophila melanogaster* RNA Pol II, recognizes an evolutionarily conserved epitope in the largest subunit RPB1 (amino acids 806–820) (Kontermann et al. 1995). Rat monoclonal antibodies 3E8 and 3E10 against Ser5P- and Ser2P-RNA Pol II, respectively, were raised against synthetic peptides containing two CTD consensus repeats (Chapman et al. 2007; Akhtar et al. 2009). In agreement with the PR concept outlined above, Figure 2 demonstrates the preferential localization of RNA Pol II on the surfaces of DAPI-stained CDs in a C127 cell nucleus using indirect immunofluorescence with a combination of Pol 3/3 and Ser2P-3E10, or Pol 3/3 and Ser5P-3E8 antibodies.

NUCLEAR TOPOGRAPHY OF NASCENT RNA, DNA, AND SER2P POL II STUDIED WITH 3D-SIM

Figure 3A shows the nuclear topography of nascent RNA, immunodetected after a 7-min BrUTP pulse performed by scratch-labeling (Schermelleh et al. 2001), together with Ser2P-RNA Pol II. As expected in the light of the findings described above, discrete focal RNA signals were preferentially found at the periphery of DAPI-stained CDs. Ser2P-RNA Pol II signals showing a partial overlap with nascent RNA may signify transcripts caught *in status nascendi*. Interestingly, a complete overlap of Ser2P-RNA Pol II and nascent RNA signals is rarely seen in 3D-SIM images, in contrast to the much more frequent findings of these signals showing a side-by-side topography or being fully separated from each other. These observations are in line with the assumption that growing transcripts are released into the periphery of a transcription complex. Isolated nascent RNA signals may represent RNA Pol II transcripts fully released from the transcription machinery or, in case of nucleoli, represent transcripts produced by RNA Pol III. Because Ser2P-RNA Pol II is enriched at 3′ ends of genes, isolated Ser2P-RNA Pol II signals without associated nascent RNA may represent RNA Pol II pausing at the end of transcribed genes after the release of the transcribed RNA.

In a further experiment, scratch-labeling was used to make C127 cells accessible for the uptake of both BrUTP and ATTO 488-dUTP (15-min pulse) to visualize nascent RNA and nascent DNA simultaneously in cells during S phase. Figure 3B demonstrates the presence of nascent DNA in the PR of an early S-phase nucleus. This finding provides further evidence that this compartment is also responsible for DNA replication. With increasing pulse time, we note more overlap of ATTO 488-dUTP-labeled DNA with the interior of chromatin domains, suggesting chromatin movements between the surface and the interior of CDs (data not shown; see also below) as previously found in electron microscopic studies (Jaunin et al. 2000; Jaunin and Fakan 2002). Future studies are presently under way to address in more detail the spatiotemporal organization of DNA replication. Sites of transcription and DNA replication are typically fully separated (Hughes et al. 1995; Wei et al. 1998; Malyavantham et al. 2008a,b). In agreement with 3D-SIM, spatially modulated illumination (SMI) microscopy revealed 125 nm as an average diameter of replication foci with a size range between 40 and 210 nm. This size range was conserved throughout S phase and yielded threefold to fivefold more distinct replication foci than previously reported (Baddeley et al. 2009).

NUCLEAR TOPOGRAPHY OF SER5P-RNA POL II AND HISTONE H2B-GFP STUDIED WITH SPDM

Next, we have used two-color SPDM for "nanoimaging" the spatial distribution of Ser5P-RNA Pol II in HeLa cells stably expressing histone H2B-GFP (Fig. 4). Specimens were illuminated and imaged as described by Gunkel et al. (2009). Results of a quantitative evaluation of SPDM images (Fig. 5) suggest that the RNA Pol II distribution clearly deviates from a random distribution. As a caveat, one needs to take into account that Ser5P-RNA Pol II molecules were detected by indirect immunofluorescence using secondary antibodies conjugated to Alexa 568 (see "Considerations on Methodological Limitations"). To investigate quantitative properties of RNA Pol II clusters, we determined for each Alexa 568 signal the number of neighboring Alexa 568 signals within a radius of 100 nm (Fig. 5A). Signal accumulations were considered as clusters suggesting a TF, when they met the following criteria: (1) at least five signals were located within a radius of 50 nm of a chosen reference signal; (2) signal counts around the reference signal revealed a peak followed by a sharp drop suggesting a border. Using these criteria, we found that most clusters contained 20–30 Alexa 568 fluorophore signals. As a limitation of these findings, it should be noted that the sample volume of signals included the entire depth of a given optical section (~600 nm). To overcome this limitation, we are currently applying SPDM to ultrathin nuclear sections. Figure 5B shows that the mean distance between two Alexa 568 signals within a cluster is 15.5 ± 4.5 nm, whereas the mean localization accuracy of an individual signal is ~22 nm. From these data, we estimate an overall structural resolution of 27 nm. Figure 5C indicates an average diameter of RNA Pol II clusters of ~100 nm with diameters of individual clusters ranging from 40 to 198 nm. Our analysis cannot exclude the existence of smaller clusters. However, in order to detect them, a much higher density of signals must be recorded, and more sophisticated quantitative evaluation procedures must be developed (Bohn et al. 2010).

Martin et al. (2004) used the monoclonal mouse antibody H5 directed against Ser2P-RNA Pol II to visualize TFs. Size measurements were carried out both with transmission electron microscopy (TEM) and spatially modulated illumination (SMI) microscopy, another type of super-resolution fluorescence microscopy particularly suited for accurate size measurements of fluorescent objects in the order of 40–100 nm (Baddeley et al. 2009; Cremer et al. 2010). Using TEM, Martin et al. (2004) determined a mean diameter of 45 nm for potential TFs, whereas SMI microscopy yielded a mean diameter for factories of ~80 nm. Eskiw et al. (2008) used electron spectroscopic imaging (ESI) and found that the size of TFs ranged between 60 and 120 nm with an average of 87 nm. In summary, the results of 3D-SIM, SMI, SPDM, TEM, and ESI consistently show that typical TF sizes are well below the 200-nm resolution limit of standard fluorescence microscopes. Present differences between the outcome of different approaches must be weighted with respect to the profound methodological differences between various approaches of light optical nanoscopy and electron microscopy (see "Considerations on Methodological Limitations"). Nevertheless, all approaches have yielded a common size overlap for TFs ranging from 40 to 85 nm.

NUCLEAR TOPOGRAPHY OF HISTONE MODIFICATIONS H3K4ME3 AND H4K8AC IN RELATION TO SER2P-RNA POL II STUDIED WITH 3D-SIM

Figure 6 depicts a C127 cell interphase nucleus after double immunolabeling with anti Ser2P-3E10 together with either anti-H3K4me3 or anti-H4K8ac antibodies. These

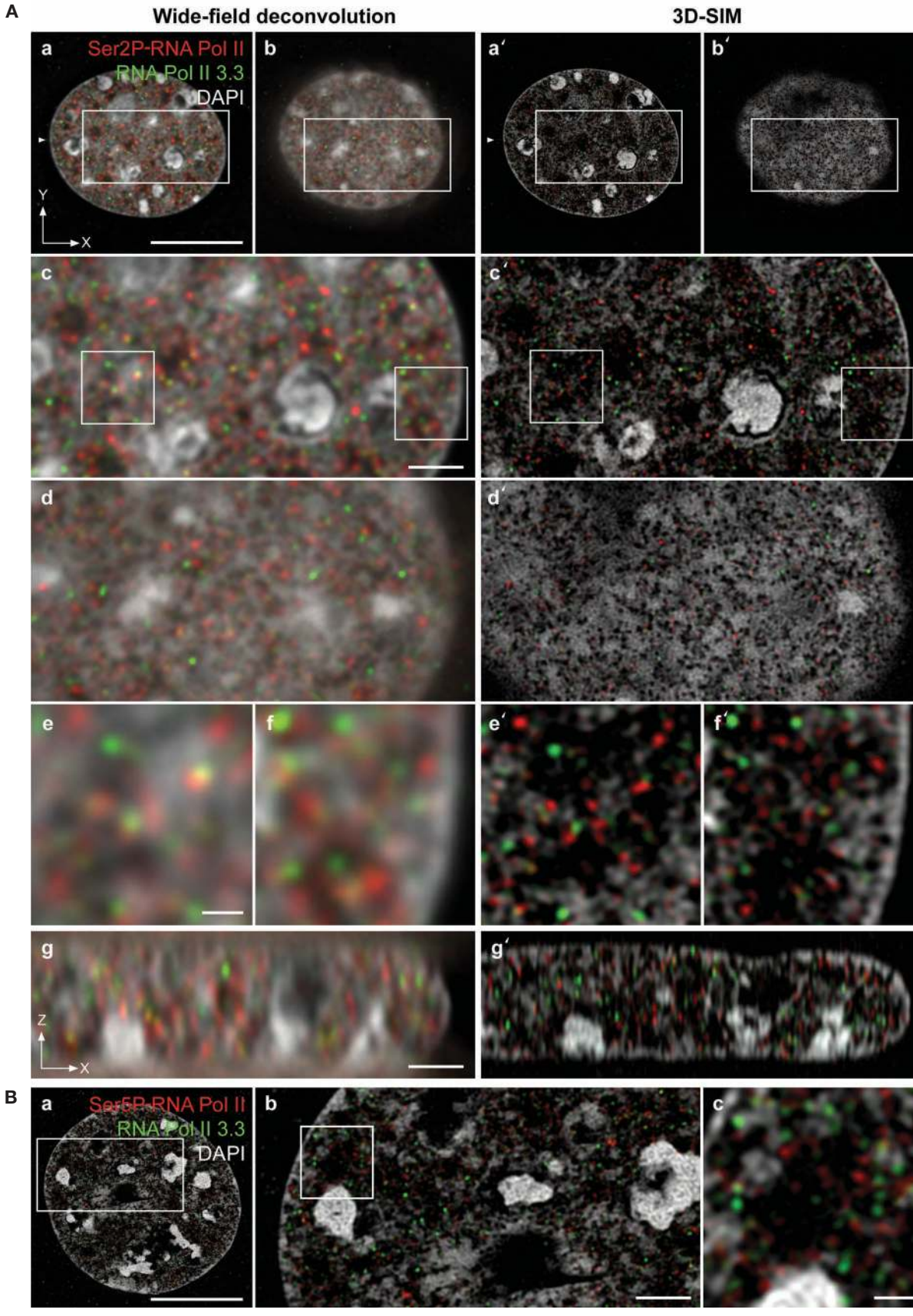

Figure 2. (*See facing page for legend.*)

histone modifications are typical for chromatin competent for transcription or in the process of transcription (Buratowski 2009). H3K4me3 has been found to be enriched at promoter regions of genes (Steiner et al. 2009; Wang et al. 2009). Ser2P-RNA Pol II (3E10) signals were typically found closer toward the IC than H3K4me3 signals. The observation that H4K8ac and, in particular, H3K4me3 modifications are highly enriched at the periphery of CDs indicates a preferential location of promoter regions as well as transcriptionally competent or active chromatin within the PR. Moreover, the lack of substantial colocalization between AT-rich DNA sequences stained with DAPI and these histone marks suggests an enrichment of GC-rich sequences within the PR. The fact that H4K8ac and H3K4me3 chromatin signatures were barely detected in the interior of IC lacunas is in agreement with the prediction of the CT-IC model that IC lacunas and wider channels (≥400 nm width) are spared from chromatin fibers, whereas in narrow IC channels, the neighboring PR regions are close enough to allow direct chromatin associations or intermingling. As mentioned above, Brownian motions of CDs also allow for transient chromatin contacts that may be stabilized and become permanent under certain conditions.

NUCLEAR TOPOGRAPHY OF SPLICING SPECKLES AND SER2P-RNA POL II STUDIED WITH 3D-SIM

Figure 7 shows the nuclear topography of splicing speckles in a human fibroblast nucleus probed with mouse-anti-SC-35 antibodies (Albiez et al. 2006). Nuclear speckles were first discovered by electron microscopists and termed "interchromatin granule clusters." The preferential distribution of speckles in the interior of the IC noted in our present study is in line with previous EM studies (Monneron and Bernhard 1969; von Schack et al. 1993). A recent study performed with laser scanning microscopy took advantage of the possibility to manipulate the condensation of CDs and the width of the IC in living cells in a fully reversible manner by the transient incubation of cells in hyper-osmolar medium (Albiez et al. 2006). Notably, splicing speckles and nuclear bodies are mainly detected in IC lacunas with a width ≥400 nm.

FUNCTIONAL INTERACTIONS BETWEEN THE INTERIOR OF CHROMATIN DOMAINS AND THE PERICHROMATIN REGION

Our failure to detect essential components for transcription in the interior of CDs does not result from a limited accessibility to primary or secondary antibodies. Other studies showed the penetration of antibodies detecting transcriptionally silent chromatin into condensed chromatin, such as antibodies against histone methyl marks (Zinner et al. 2006) or primate-specific histone variants H3.X and Y (Wiedemann et al. 2010). Furthermore, the formation of nascent RNA and nascent DNA in the PR is in line with evidence obtained by transmission electron microscopy (TEM) using a postembedding immuno-gold protocol (Jaunin and Fakan 2002; for review, see Rouquette et al. 2010). Here, cells were fixed with glutaraldehyde under conditions seemingly appropriate for a high structural preservation and embedded in resin. Immunogold detection was performed on ultrathin sections. This approach allowed the binding of primary antibodies only to epitopes exposed at section surfaces. Thus permeation problems, which may limit studies of complete cells, were excluded. EM studies using short pulses with labeled nucleotides, as well as pulse-chase experiments, revealed DNA replication sites in the PR (Fakan and Hancock 1974; Jaunin et al. 2000; Jaunin and Fakan 2002). These studies demonstrated that segments of chromatin prone for replication expand into the PR, became replicated, and were subsequently relocated into the interior of CDs. In HeLa cells, DNA replication was reported to take place in nuclear body-like structures called replication factories (Hozák et al. 1994; Philimonenko et al. 2006).

With regard to transcription, dynamic interactions between the PR and the interior of CDs are expected, but speculative at this stage. Two scenarios may be considered:

Scenario I: All coding DNA sequences and regulatory sequences located at 5′ and 3′ ends of a given gene are present in toto in the PR independent of their current transcriptionally active or silent state.

Scenario II: DNA sequences to be transcribed are only in part present in the PR, whereas the major part of a given gene is embedded as condensed chromatin in the interior of CDs (Rouquette et al. 2010). This scenario argues for a transcription process working hand in hand with a very dynamic decondensation and recondensation process of a gene's chromatin in a sequential, stepwise manner. Accordingly, transcription would involve highly dynamic local chromatin events albeit at scales that cannot be resolved by conventional light microscopy. Initially, the promoter region may provide an address within the PR necessary to initiate transcription. At this point, the first 5′ segment of the gene becomes exposed in the PR as a fully decondensed segment, whereas the majority of the gene is still embedded within the compact interior of the CD. Whereas a segment of exons and/or introns is tran-

Figure 2. Nuclear topography of RNA Pol II visualized with wide-field fluorescence microscopy and 3D-SIM. (*A*) Comparison between optical sections from a C127 cell nucleus obtained from deconvolved conventional wide-field images (*a*–*g*) and 3D-SIM images (*a*′–*g*′). Ser-2P RNA Pol II (red) and Pol 3/3 (green) primary antibodies were used to mark the CTD domain repeats phosphorylated at serine 2, and the RPB1 domain of the enzyme, respectively, together with secondary antibodies conjugated to Alexa 594 (red) and Alexa 488 (green). DNA was counterstained with DAPI (gray). (*a*,*a*′) Equatorial nuclear section. (*b*,*b*′) Apical lateral (*x*, *y*) nuclear section. Bar, 10 µm. (*c*,*c*′) 3× Magnified boxed region in *a* and *a*′. (*d*,*d*′) 3× Magnified boxed region in *b* and *b*′. Note that chromatin pores in *b*′–*d*′ reflect IC channels expanding through chromatin located beneath nuclear pores and the lamina. Bar, 2 µm. (*e*,*f*,*e*′,*f*′) 3× Magnified, boxed regions from *c* and *c*′. Bar, 500 nm. (*g*,*g*′) Axial (*x*, *z*) midsection. Bar, 2 µm. (*Ba*) Light optical section of a C127 cell nucleus obtained with 3D-SIM image after indirect immunolabeling with anti-Ser-5P RNA Pol II (red) and anti-RNA Pol 3/3 (green) antibodies and counterstained with DAPI (gray). Bar, 10 µm. (*b*) 3× Magnification of region marked in *a*. Bar, 2 µm. (*c*) 3× Magnification of region marked in *b*. Bar, 500 nm. Note that RNA Pol II signals are highly enriched in the perichromatin region (PR) in contrast to their sparse occurrence or entire lack in the interior of IC lacunas.

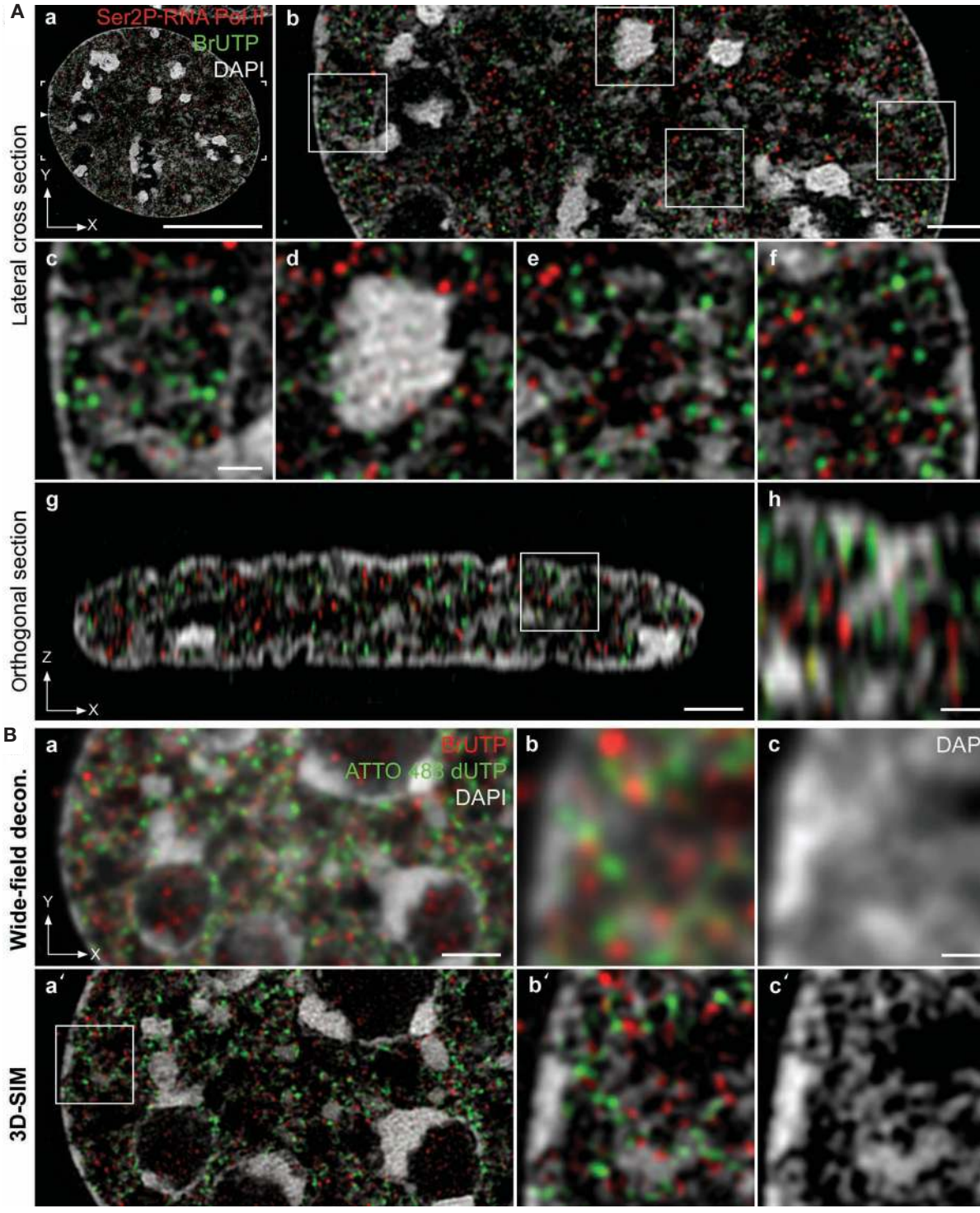

Figure 3. Nuclear topography of nascent RNA, nascent DNA, and Ser2P-RNA Pol II. (*a*) Lateral (*x*, *y*), optical section recorded with 3D-SIM from a DAPI-stained (gray) C127 cell nucleus, fixed after a 7-min scratch labeling pulse with BrUTP, shows nascent RNA (green) and Ser2p-RNA Pol II (red). Indirect immunofluorescence was performed with specific primary antibodies against B-labeled epitopes and serine-2-phosphorylated CTD, respectively, followed by secondary antibodies conjugated to Alexa 594 (red) and to Alexa 488 (green), respectively. Bar, 10 µm. (*b*) 3× Magnification of region marked in *a*. Bar, 2 µm. (*c–f*) 3× Magnification of four regions marked in *b*. Bar, 500 nm. (*g*) Axial, midsection (*x*, *z*) of the same nucleus. Bar, 2 µm. (*h*) 3× Magnification of region marked in *g*. Bar, 500 nm. Note the enrichment of nascent RNA and Ser2P-RNA Pol II signals at the periphery or on fibrillar protrusions of CDs. Note that most nascent RNA is synthesized in the PR consistent with the localization of RNA Pol II in the PR but not in the interior of IC lacunas. (*Ba*,*a′*) Partial views of a lateral (*x*, *y*) optical midsection from a C127 cell nucleus obtained with conventional wide-field deconvolution (*a*) and 3D-SIM (*a′*) show the topography of nascent RNA (red) and nascent DNA (green) in the context of DAPI-stained DNA (gray). Bar, 2 µm. The nucleus was fixed 15 min after a scratch-labeling pulse with both BrUTP and dUTP, directly conjugated to the fluorescent dye ATTO 488 (green). B-labeled epitopes in newly synthesized RNA were detected by indirect immunofluorescence with specific primary antibodies and secondary antibodies conjugated to Alexa 594 (red). (*b*,*b′*) 3× Magnification of the region marked in *a′*. (*c*,*c′*) The same region with DAPI-stained DNA only. Bar, 500 nm. Note that both nascent DNA and nascent RNA were synthesized in the PR, but not in the interior of IC lacunas.

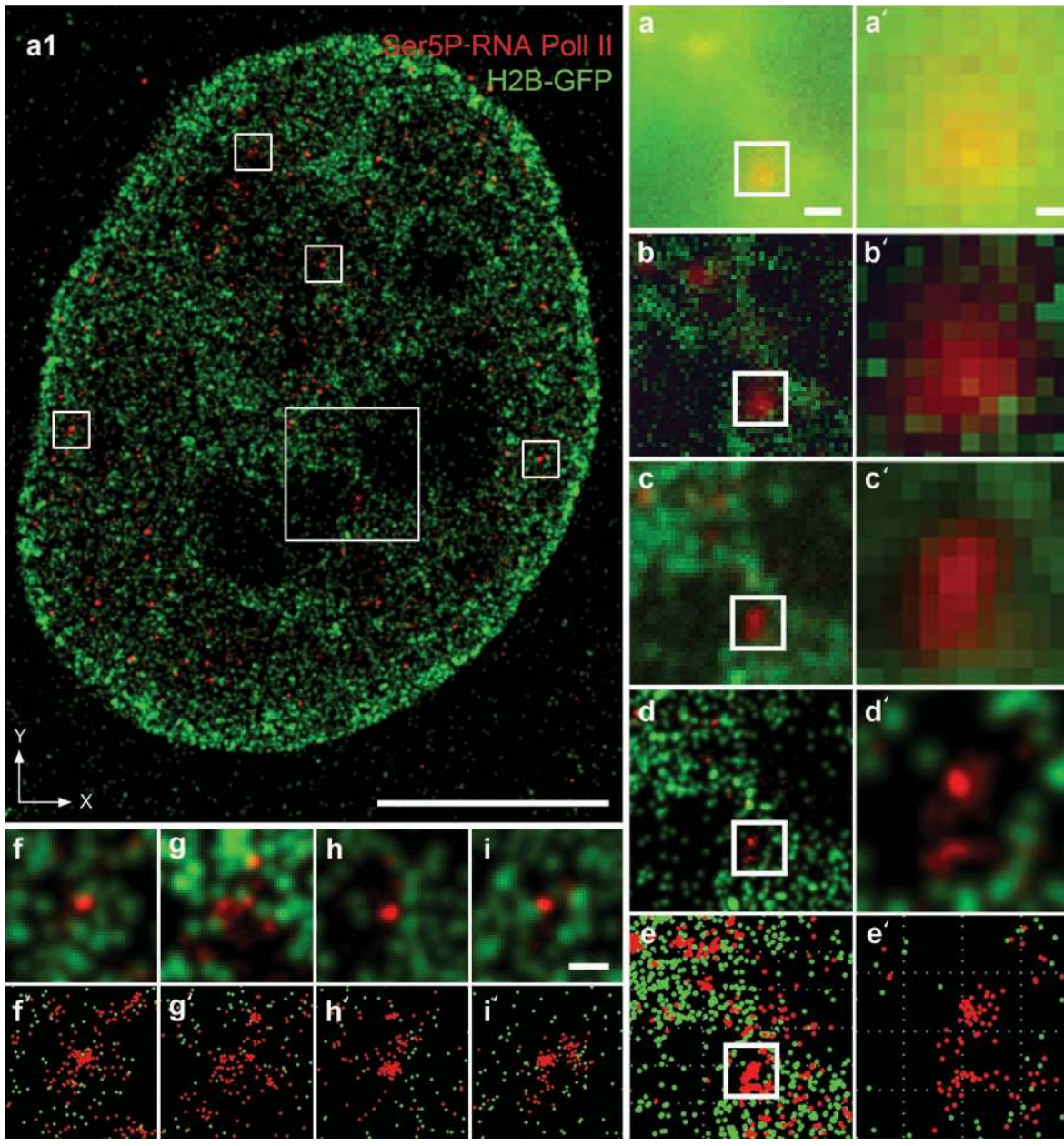

Figure 4. Nuclear topography of Ser5P-RNA Pol II and histone H2B studied with SPDM. (*a1*) Two-color SPDM image from a light optical plane through a HeLa cell nucleus. Ser5P-RNA Pol II was detected with specific primary and secondary antibodies conjugated to Alexa 568 (red). H2B-GFP was detected with anti-GFP and secondary antibodies conjugated to Alexa 488 (green). Bar, 10 µm. The image was blurred with a Gaussian kernel corresponding to the estimated mean localization accuracy of individual photon emitting, that is, "blinking," fluorophores of ~20 nm (for details, see Gunkel et al. 2009). (*a–e*) Magnifications of the region marked by the large box in *a1*. Bar, *a,* 500 nm. (*a′–e′*) Further magnification of the regions marked by a box in *a–e*. Bar, *a′*, 100 nm. These images allow a comparison of the resolution obtained with conventional wide-field epifluorescence microscopy before (*a*,*a′*) and after processing with a high-pass filter to reduce background (Jähne 2005) (*b*,*b′*) (NA = 1.4, λ = 520 nm, resulting in an FWHM of ~200 nm) with the resolution of SPDM (*c–e* and *c′–e′*). (*c*,*c′*) For comparison with *b* and *b′* the SPDM images shown in *d* and *d′* were convoluted with a simulated conventional wide-field PSF (Point Spread Function) with added background noise. (*d*,*d′*) In this image, individual positions of "blinking" fluorophores were blurred with Gaussian kernels corresponding to the localization accuracy of these signals, emphasizing the potential of SPDM to localize individual proteins of interest via conjugated fluorophores. (*e*,*e′*) Positions of single fluorophores represent the peaks of the Gaussian approximation calculated from the photons emitted from each individual "blinking" fluorophore (for further explanation, see Fig. 9 in Cremer et al. 2010). Note that *b′* shows an empty resolution, notwithstanding attempts of digital improvement, whereas *e′* resolves the positions of individual, "blinking" fluorophores. (*f–i*,*f′–i′*) Enlargements of four regions marked by small boxes in *a1* (bar, 100 nm) indicate additional clusters of Ser5P-RNA Pol II (cf. *d′* and *e′*).

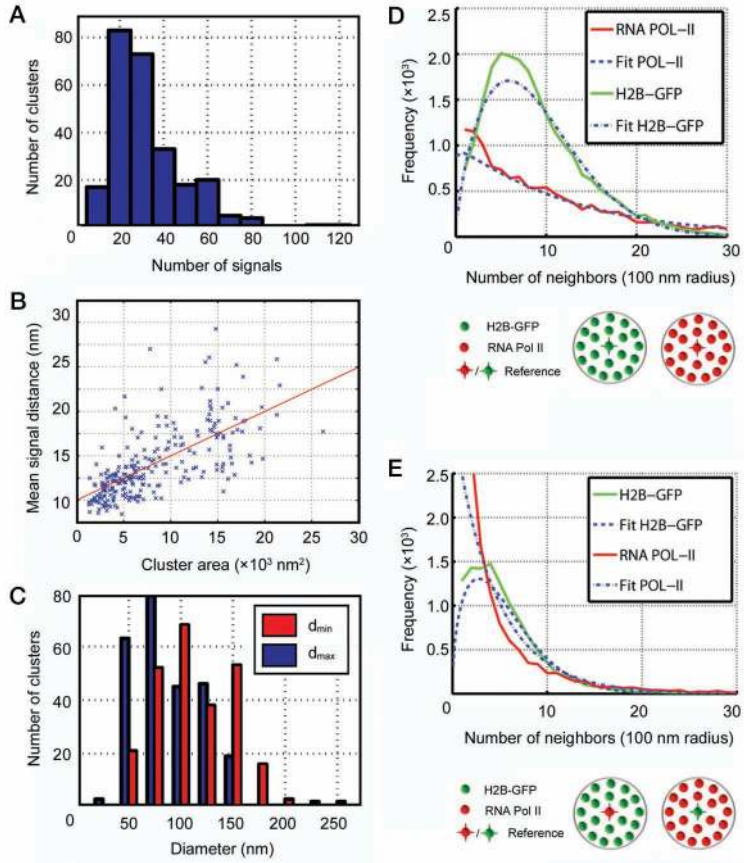

Figure 5. Quantitative evaluation of SPDM images. (*A*) The histogram shows the frequency of clusters with different numbers of Ser5P-Pol II signals (range: ~10–80 signals per cluster; mean value: 33.1 ± 17.0 signals per cluster) detected by indirect immunofluorescence using secondary antibodies conjugated to Alexa 568 (cf. Fig. 4; see text for further explanation on cluster determination). Although it seems reasonable to correlate the signal of a single, blinking Alexa 568 fluorophore with a single RNA Pol II molecule, two caveats complicate this interpretation. First, the presence of some noninformative signals due to unspecific binding of Alexa 568–tagged, secondary antibodies, could result in an overestimation of nonclustered Ser5P-Pol II. Second, because anti-Ser5P-Pol II antibodies may bind to several of the 52 repeats present in a single CTD, the exact relationship between signal counts and the number of RNA Pol II molecules is presently not known. (*B*) Mean distance between single, mapped Alexa 568 fluorophores, arguably representing the localization of single RNA Pol II molecules, as a function of the cluster area and density. *x* axis: Total area measured for each RNA Pol II signal cluster; *y* axis: mean signal distance per cluster. For these data, an average signal localization accuracy of 22 nm was determined. (*C*) Histograms show the estimated minimum (d_{min}: blue) and maximum (d_{max}: red) diameters of detected RNA Pol II clusters. Only clusters exhibiting a normal signal distribution were included in these measurements. Mean d_{min} value: 87 nm (±30 nm); mean d_{max} value: 112 nm (±39 nm). The data indicate an average size of 100 nm (±33 nm) for these clusters with a range from 40 to 198 nm. (*D*) Distribution of H2B-GFP and Ser5P-RNA Pol II signal densities. The red curve delineates the number of RNA Pol II neighboring signals counted within a 100-nm radius around a given RNA-Pol II signal, the green curve the number of neighboring H2B-GFP signals counted within a 100-nm radius around a reference H2B-GFP signal. The circle marked by an asterisk in the schemes below represents the central molecule of reference surrounded by the same type of neighboring molecules. (*E*) Correlation of H2B-GFP and Ser5P-RNA Pol II signal densities. The red curve delineates the number of RNA Pol II neighboring signals counted within a 100-nm radius around a given H2B-GFP signal. The green curve depicts the number of H2B-GFP signals counted within a 100-nm radius around Ser5P-RNA Pol II signals. Schematic representation of examples for each type of measurement. In the schemes below, the circle marked by an asterisk represents the central molecule of reference surrounded by a different type of neighboring molecules. Our data suggest that increased densities of RNA Pol II are associated with decreased densities of H2B and—in connection with the enrichment of RNA Pol II in the PR (cf. Figs. 2, 3, 7)—support a decreased chromatin condensation in the PR.

scribed, the next segment of the gene is becoming fully decondensed and located into the PR. Transcribed DNA segments are rapidly reconfigured into a higher-order chromatin compaction and relocated into core chromatin beneath the PR. Moreover, it seems possible that silent genes together with their promoter region are fully embedded in the interior of CDs. This hypothesis implies that the transcriptional activation of a fully inactive gene requires its translocation to the PR as a first step.

FUNCTIONAL INTERACTIONS BETWEEN THE PERICHROMATIN REGION AND THE INTERCHROMATIN COMPARTMENT

We hypothesize that the IC is the nuclear compartment that provides the necessary supply of factors for transcription, cotranscriptional splicing, DNA replication, and repair to the PR (Rouquette et al. 2010). Splicing speckles, for example, located in the interior of the IC are a storage

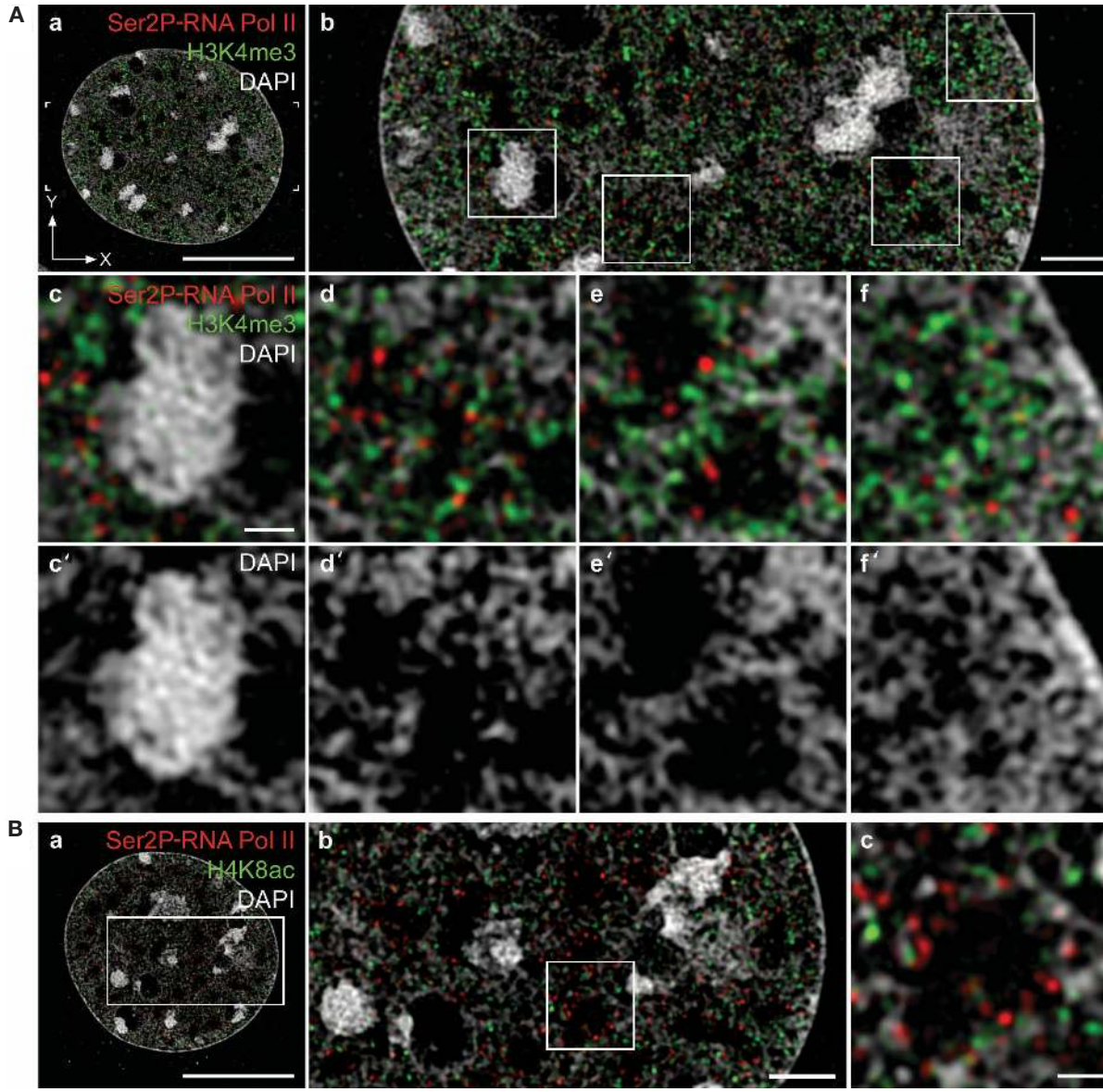

Figure 6. Nuclear topography of histone modifications H3K4me3 and H4K8ac in relation to Ser2P-RNA Pol II. (*Aa*) 3D-SIM optical section from a DAPI-stained (gray) C127 cell nucleus following immunodetection of Ser2P-RNA Pol II (red) and H3K4me3 (green) with specific primary antibodies and secondary antibodies conjugated to Alexa 594 (red) and to Alexa 488 (green), respectively. Bar, 10 µm. (*b*) 3× Magnification of the region marked in *a*. Bar, 2 µm. (*c–f*) 3× Magnification of regions marked in *b*; (*c′–f′*) same images with DAPI staining only. Bar, 500 nm. (*Ba*) 3D-SIM optical section from a DAPI-stained (gray) C127 cell nucleus following Ser2P-RNA Pol II (red) and H4K8ac (green) immunodetection with specific primary antibodies and secondary antibodies conjugated to Alexa 594 and to Alexa 488, respectively. Bar, 10 µm. (*b*) 3× Magnification of the region marked in *a*. Bar, 2 µm. (*c*) 3× Magnification of region marked in *b*. Bar, 500 nm. Note that both H3K4me3- and H4K8ac-modified nucleosomes are enriched in the PR in addition to RNA Pol II, but excluded from the interior of IC lacunas.

site of transcription factors. These factors migrate by diffusion to the PR and provide the necessary supply for cotranscriptional RNA splicing. Spliced and protein-packaged mRNAs are then released into the IC, which may also provide the essential compartment for the export of ribonucleoproteins (RNPs) to the nuclear periphery, where IC channels end at nuclear pores. Nuclear bodies, such as PML bodies located in the IC, may also provide factors to initiate and/or maintain transcription going on in the PR (Tashiro et al. 2004).

PERICHROMATIN REGION AND NUCLEAR MATRIX

Our data suggest that scaffold/matrix attachment regions (S/MARs), which establish loop domains and have a key role in priming regions of the genome for transcription (Linnemann et al. 2009), are located in the PR. A nuclear matrix has been proposed as "the site of organization for replication, transcription and posttranscriptional processing" (Berezney and Coffey 1975; Berezney et al. 1995).

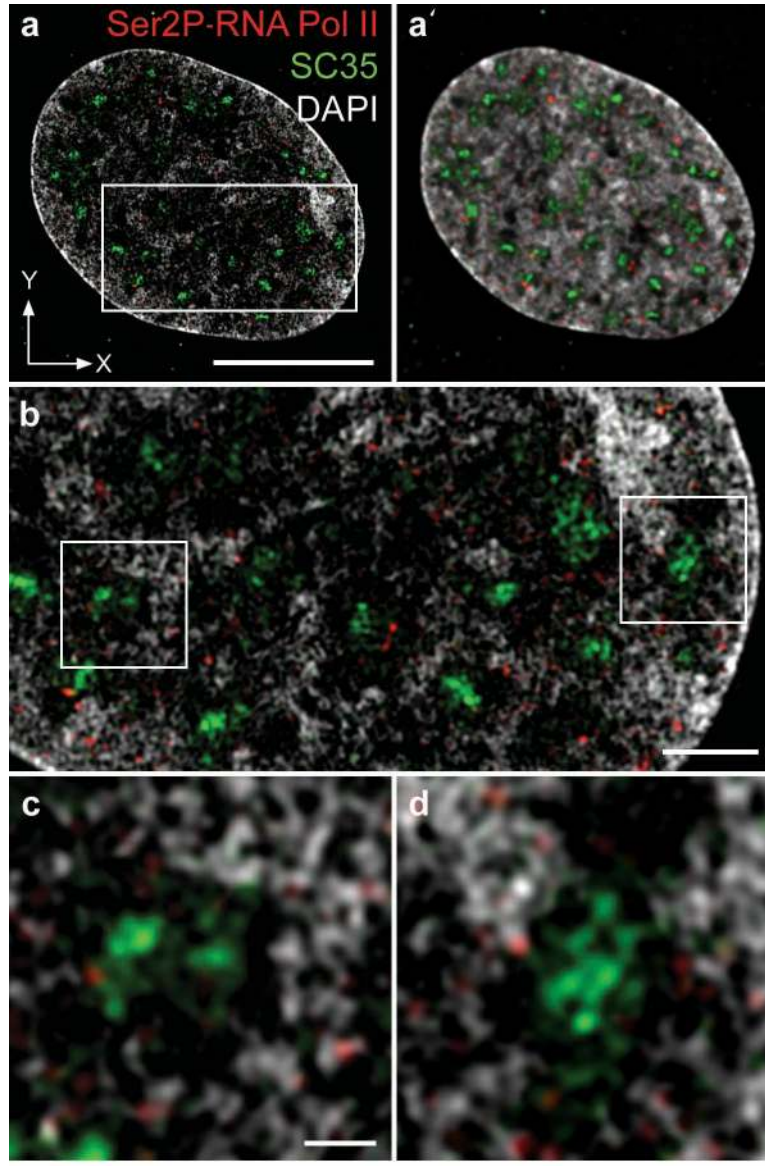

Figure 7. Nuclear topography of splicing speckles and Ser2P-RNA Pol II. (*a*) 3D-SIM optical section and (*a′*) wide-field deconvolved section of a DAPI-stained (gray) human fibroblast. Ser2P RNA Pol II (red) and SC-35 (green) were immunodetected with specific primary antibodies and secondary antibodies conjugated to Alexa 594 (red) and to Alexa 488 (green), respectively. Bar, 10 µm. (*b*) 3× Magnification of the region marked in *a*. Bar, 2 µm. (*c*,*d*) 3× Magnification of the two regions marked in *b*. Bar, 500 nm. Note that splicing speckles are typically located in the interior of IC lacunas in contrast to the preferential localization of RNA Pol II in the PR.

The nuclear matrix concept emphasizes a framework of branched 10-nm-thick core filaments (Nickerson et al. 1997), to which proteins involved in major nuclear functions are directly or indirectly attached. Proteins generating the core filaments, however, have not been identified so far despite considerable efforts. Nevertheless, a dynamic nuclear matrix may help to organize the complex biochemistry involved in major nuclear functions. The nuclear matrix proteome has been "operationally defined as the proteins from cells and tissue that are extracted following a specific biochemical protocol; in brief, the soluble proteins and lipids, cytoskeleton, and chromatin elements are removed in a sequential fashion, leaving behind the proteins that compose the NM" (Albrethsen et al. 2009). This biochemical nuclear matrix is exceedingly variable in its protein composition. Rather than being a rigid, invariant nuclear skeleton involved in the arrangement of CTs (Hubert and Bourgeois 1986), the core matrix may represent a "dynamic sponge with open compartments for free diffusion in the nucleoplasm…" (Donald S. Coffey; quoted in Albrethsen et al. 2009). Considering the sponge-like architecture of CTs, built up from interconnected CDs and pervaded by IC channels, we argue that one should search for such a core matrix in the PR. A core matrix may be built up and degraded locally depending on its role in the structural organization of various essential functions taking place in the PR. Given the still questionable nature of a core matrix, its actual contribution in nuclear function and

possibly also in higher-order chromatin organization remains to be seen. Large-scale chromatin structures may rather be a problem of chromatin self-organization (Sinclair et al. 2010).

TRANSCRIPTION AND DNA REPLICATION: A CASE OF FUNCTIONAL NUCLEAR ARCHITECTURE IN MOTION

We consider the PR as the nuclear compartment where chromatin replication, transcription, cotranscriptional splicing, and DNA repair take place (Solimando et al. 2009; Rouquette et al. 2010). These functions require dynamic interactions between the interior of CDs and the PR. Although movements of transcription and replication machineries, respectively, along DNA strands cannot be ruled out, it seems more likely that these machineries are fixed within the PR, whereas DNA is moving (Cook 2010). To which extent nuclear structure may beget nuclear functions or, alternatively, to which extent nuclear functions may prime nuclear structure, is an old, still unanswered question. Although we consider some evidence for or against either case below, we think that the problem may reflect our desire for simple cause-and-effect solutions. In reality, linear cause-and-effect models may turn out to be invalid, giving way to network concepts of interconnected causes and effects, where effects directly or indirectly retroact on their causes.

Does Structure Beget Function?

Differential arrangements of early-replicating chromatin in the nuclear interior and mid-replicating chromatin at the nuclear periphery have been noted in evolutionary distant species ranging from humans to single-cell eukaryotes. The heterochromatic, transcriptionally inert micronuclei of the ciliate *Stylonychia lemnae* provide a case in point where this organization can be demonstrated during S phase despite the absence of transcription. All coding RNAs necessary for the synthesis of proteins involved in chromatin replication in the transcriptionally inert micronucleus are provided by the transcriptionally active macronucleus. Replication occurs in foci-like structures showing spatial and temporal patterns similar to the replication of ~1-Mb CDs in nuclei of higher eukaryotes (Postberg et al. 2005, 2008).

Does Function Beget Structure?

The transcription of ribosomal genes (by RNA Pol I) and of tRNA genes (by RNA Pol III) results in specific changes of their topography with respect to the nucleolus. Notably, these topographical changes are preceded by transcriptional activation. Accordingly, these genes provide paradigms for the hypothesis that transcription may be involved as a causal factor in the establishment of specific patterns of higher-order chromatin organization.

Gene clustering has recently been observed for the tRNA genes in *Saccharomyces cerevisiae*, where 274 tRNA genes are arranged at the nucleolus. This arrangement depends on the transcriptional activity of tRNA genes. Transcriptionally activated, but not transcriptionally silent tRNA genes are translocated from the periphery of the nucleus to the surface of the nucleolus (Haeusler and Engelke 2006).The nucleolus is also a prominent example for clustering of genes for ribosomal RNA (rRNA). Ribosomal genes are transcriptionally repressed during mitosis. Immediately after mitosis, transcription of ribosomal genes is reactivated, and specific nucleolar structures are established at each gene cluster resembling small nucleoli. Experiments in yeast have revealed that the active transcription of ribosomal genes is an indispensable, but probably also sufficient prerequisite for the formation of nucleolar structures including (1) the fibrillar center (FC), the place of rRNA transcription; (2) the surrounding dense fibrillar component (DFC) where rRNA maturation takes place; and (3) the granular component (GC), for ribosome assembly and transport to the nucleoplasm. Ribosomal genes displaced to other chromosomes can participate in the nucleolus formation, only if these genes are transcriptionally active (Trumtel et al. 2000). Apparently, the merge of several small nucleoli into a large nucleolus occurs mainly at the level of the GC structure, whereas ribosomal gene clusters from different chromosomes remain largely separated. Because genomic DNA has not been detected so far in the GC structure, it is tempting to speculate that transcripts derived from the rRNA gene locus, and/or proteins binding to these RNAs, could be critically involved in the formation and maintenance of the merged GC structure of large nucleoli.

Whereas RNA Pol I– and Pol III–transcribed genes provide support for the hypothesis that transcriptional events may cause a reorganization of certain features of the nuclear architecture, only little is known so far for RNA Pol II–transcribed genes. The transcriptome of Pol II is much more complex compared to the transcriptomes of RNA Pol I and RNA Pol III. Nuclear distribution patterns of Ser5P-RNA Pol II studied by SPDM underline the possibilities of quantitative measurements, but our study should still be considered as work in progress. At face value, our present SPDM analysis suggests that only ~10% of Ser5P-RNA Pol II molecules were present in bona fide TFs. Accordingly, most genes may be transcribed outside TFs. Although comparisons with results from other groups depend to some extent on the criteria used for the definition of TFs, such a conclusion would be in conflict with previous studies from Cook and coworkers, who have argued that ~95% of transcription may be carried out within TFs (Faro-Trindade and Cook 2006; Cook 2010). As a caveat of the present study, we emphasize that RNA Pol II was detected by indirect immunofluorescence. Accordingly, the analyzed patterns reflect the localization of fluorophore conjugated secondary antibodies. Imaging procedures able to record single emitting fluorophores are extremely sensitive to background and require the removal of nonspecifically bound secondary antibodies as completely as possible. Although we took care to wash preparations extensively after each immunodetection step, we reserve a final statement until further imaging studies with SPDM are completed. Artifacts due to nonspecifically bound primary or secondary antibodies can be overcome by the direct conjugation of a fluorophore to a nuclear protein of interest.

CONCLUSIONS AND FUTURE PROSPECTS

We examined the nuclear topography of DNA, nascent RNA, and nascent DNA, as well as RNA Pol II and histone modifications typical for transcriptionally competent/active chromatin. Observations with 3D-SIM demonstrate a strong enrichment of these components both at the surface of CDs and on occasional chromatin fibers expanding into the IC. We hypothesize that the functional nuclear organization of transcription and DNA replication occurs in the PR and depends on dynamic interactions between the exposure of transcriptionally silent chromatin located in the interior of CDs and CD surfaces, whereas the IC serves as a storage site for the supply of proteins essential for transcription, cotranscriptional splicing, and other functions going on in the PR. The IC may also serve as a special compartment for RNA export, as indicated by IC channels ending at the nuclear pores (Schermelleh et al. 2008; this study). At this point, however, we do not know whether RNPs can penetrate efficiently even through condensed chromatin and thus find their way to nuclear pores independently of the IC system. In case a decisive role for large-scale movements of CDs and loops or even entire CTs can be further substantiated, we need to figure out whether Brownian motions are sufficient for an explanation or whether mechanisms for directed movements must be involved (Strickfaden et al. 2010, 2011).

Our study shows that narrow IC channels can be filled with decondensed chromatin representing the PRs from two closely neighboring CDs, whereas the interior of IC lacunas is the home of splicing speckles and likely also of certain nuclear bodies but is spared from chromatin. This observation argues that differences between the CT-IC model and the ICN model with respect to the problem of chromatin intermingling are to some extent a question of scale rather than principle. Present evidence demonstrates the importance of the PR and IC as functionally relevant nuclear compartments, which should be distinguished from the compact interior of CDs. Arguably, the PR constitutes the euchromatic nuclear compartment, whereas the interior of CDs constitutes a heterochromatic compartment. For better understanding of higher-order chromatin organization, it is important to distinguish between giant chromatin loops, which may deeply invade into a neighboring CT or even connect widely separated CTs in *trans*, and small-sized chromatin loops invading the PR. A genome-wide approach for quantitative measurements of chromatin loop sizes and chromatin loop compaction in different cell types would be helpful for this purpose.

Considerations on Current Methodological Limitations and Future Improvements

Because each microscopic approach has its own advantages and disadvantages, correlative microscopy provides the best chance for reliable results (for reviews, see Rouquette et al. 2010; Schermelleh et al. 2010). Correlative microscopy implies the sequential use of different approaches to study the same cell first in its living and then in its fixed state. 3D-structured illumination microscopy provides images with a resolution down to 100 nm, whereas spectrally assigned localization microscopy has made it possible to localize high numbers of individual, fluorophore-tagged macromolecules with nanometer accuracy. Whereas simple intensity thresholding can often be conveniently used to remove "diffuse" background in conventional fluorescence microscopic images, this is not possible in the case of single-molecule detection procedures. A solution of this problem requires the development of new ways of thresholding, for example, based on the local density of signals.

Fixation artifacts are a nightmare for every microscopist, as they may lead to structural changes compared with the in vivo situation. TEM using postembedding protocols is presently superior in resolution, but conclusions are sometimes complicated because of the typically sparse label density of gold grains. The use of specimens prepared by rapid cooling for cryo-EM bears the promise that the topography of all molecules in the specimen is maintained in a close-to-native state. Whereas EM is principally limited to studies of fixed cells, we expect that several, next-generation approaches of light optical nanoscopy will allow studies of living cells with nanometer resolution at the level of single fluorophore-tagged macromolecules.

Understanding Nuclear Architecture Requires a Combination of High-Throughput Molecular Studies with Super-Resolution Microscopy in Space and Time

Older images depicting higher-order chromatin organization tended to show chromatin as an unordered network of intermingling chromatin fibers, whereas recent ones take into account compelling evidence for specific chromatin interactions in *cis* (within a given CT) and in *trans* (between different CTs) derived from chromosome conformation capture (3C) approaches (Dekker et al. 2002; de Laat and Grosveld 2007; Osborne et al. 2007). In combination with high-throughput sequencing, a recent improvement of this method, termed Hi-C, has allowed mapping of DNA–DNA interactions in *cis* and in *trans* at ~1-Mb resolution (Lieberman-Aiden et al. 2009). Notably, data obtained by 3C approaches are based on the statistic evaluation of such interactions in large cell numbers. The resolution of DNA–DNA interactions by Hi-C beyond 1 Mb at finer scales is possible, but requires much higher reads. The method has therefore inherent limitations, when cell numbers are small, for example, in studies of early developmental stages (Koehler et al. 2009), or in case of heterogeneous cell populations, a common problem not only in tissues but also in in vitro cell cultures. Hi-C is particularly suited to study homogeneous cell populations or basic features of nuclear organization present in diverse cell types.

Another seminal approach is the genome-wide analysis of protein–DNA interactions using chromatin immunoprecipitation combined with DNA microarrays (ChIP on Chip) (Kim and Ren 2006) or DNA adenine methyltransferase identification (DamID) (van Steensel and Henikoff 2000). The latter approach, for example, has made possi-

ble a genome-wide characterization of DNA sequences interacting with the lamina underpinning the nuclear envelope in *Drosophila melanogaster* and human cells (Kind and van Steensel 2010). Currently, a single DamID assay can be performed with ~100,000 cells and most likely with even less. Single-cell DamID may become possible, but because the Dam methylation events at any given locus are stochastic (yes or no events), such a single-cell assay would give a very noisy picture (B. van Steensel, pers. comm.).

In summary, high-throughput molecular biological approaches combined with innovative microscopic approaches provide the most promising route toward unraveling 3D (space) and four-dimensional (4D; space and time) topographical interactions of CDs with the machineries for major nuclear functions, such as transcription and DNA replication.

On the Necessity of an Evolutionary Approach to the Functional Nuclear Organization

Comparative evolutionary studies are an essential task to distinguish nuclear architectural features, which are conserved both in single-cell eukaryotes and multicellular species, from those that are species- and/or cell-type-specific (Postberg et al. 2010). Such studies should not be belittled as being only descriptive in comparison to mechanistic studies performed at the molecular level. The current wealth of molecular studies exploring the mechanisms of mitosis and cell division would not be possible without the detailed, quantitative description of this process starting in the second half of the 19th century. We need detailed, quantitative information on the possible range of nuclear phenotypes, which evolved both within and between species. Such studies provide the phenomenological basis on which mechanistic hypotheses can be developed and experimentally tested.

The evolution of the functional nuclear organization may be compared with the origins of a natural landscape (Cremer et al. 2006). The proper, cell-type-specific use of genetic information may essentially depend on a multitude of nuclear landscapes. Francois Jacob has fittingly compared evolution with a tinkerer (Jacob 1977). The evolutionary tinkerer, in contrast to a group of clever engineers, has no foresight, but is driven by unplanned mutations in the never-ending trials of modifying proteins and putting them together in unexpected ways (Alon 2003). Anything goes, which does not fall victim to the constraints of natural evolution, including not only selection, but also chance or simply bad luck. To quote Charles Darwin, "There is grandeur in this view of life," which explains the evolution of "endless forms most beautiful and most wonderful." This view enforces a detailed, quantitative description of the various nuclear landscapes that have been realized during evolution in different species and cell types. Lacking this information, we can presently not even envisage the still unexplored variability of molecular mechanisms involved in the range of functional nuclear organizations that may have been realized to date in different species and cell types.

ACKNOWLEDGMENTS

Work in the authors' laboratories has been supported by the Deutsche Forschungsgemeinschaft (DFG), the European Union, Nanosystems Initiative Munich (NIM), and the LMU BioImaging Network (BIN). T.C. is indebted to Stanislav Fakan (University of Grenoble, Switzerland) for many stimulating discussions about the concept of the perichromatin region. Discussions with Ronald Berezney (University at Buffalo, NY), Donald Coffey (Johns Hopkins University, MD) and Jeffrey Nickerson (University of Massachusetts, MA) regarding the nuclear matrix concept are also gratefully acknowledged. We thank our colleague Hilmar Strickfaden for help with image reconstructions.

REFERENCES

Ahmed K, Dehghani H, Rugg-Gunn P, Fussner E, Rossant J, Bazett-Jones DP. 2010. Global chromatin architecture reflects pluripotency and lineage commitment in the early mouse embryo. *PLoS One* **5:** e10531. doi: 10.1371/journal.pone.0010531.

Akhtar MS, Heidemann M, Tietjen JR, Zhang DW, Chapman RD, Eick D, Ansari AZ. 2009. TFIIH kinase places bivalent marks on the carboxy-terminal domain of RNA polymerase II. *Mol Cell* **34:** 387–393.

Albiez H, Cremer M, Tiberi C, Vecchio L, Schermelleh L, Dittrich S, Kupper K, Joffe B, Thormeyer T, von Hase J, et al. 2006. Chromatin domains and the interchromatin compartment form structurally defined and functionally interacting nuclear networks. *Chromosome Res* **14:** 707–733.

Albrethsen J, Knol JC, Jimenez CR. 2009. Unravelling the nuclear matrix proteome. *J Proteomics* **72:** 71–81.

Alon U. 2003. Biological networks: The tinkerer as an engineer. *Science* **301:** 1866–1867.

Baddeley D, Chagin VO, Schermelleh L, Martin S, Pombo A, Carlton PM, Gahl A, Domaing P, Birk U, Leonhardt H, et al. 2009. Measurement of replication structures at the nanometer scale using super-resolution light microscopy. *Nucleic Acids Res* **38:** e8. doi: 10.1093/nar/gkp901.

Berezney R, Coffey DS. 1975. Nuclear protein matrix: Association with newly synthesized DNA. *Science* **189:** 291–293.

Berezney R, Mortillaro MJ, Ma H, Wei X, Samarabandu J. 1995. The nuclear matrix: A structural milieu for genomic function. *Int Rev Cytol* **162A:** 1–65.

Berezney R, Dubey DD, Huberman JA. 2000. Heterogeneity of eukaryotic replicons, replicon clusters, and replication foci. *Chromosoma* **108:** 471–484.

Betzig E, Patterson GH, Sougrat R, Lindwasser OW, Olenych S, Bonifacino JS, Davidson MW, Lippincott-Schwartz J, Hess HF. 2006. Imaging intracellular fluorescent proteins at nanometer resolution. *Science* **313:** 1642–1645.

Bohn M, Diesinger P, Kaufmann R, Weiland Y, Muller P, Gunkel M, von Ketteler A, Lemmer P, Hausmann M, Heermann DW, et al. 2010. Localization microscopy reveals expression-dependent parameters of chromatin nanostructure. *Biophys J* **99:** 1358–1367.

Bouchet-Marquis C, Dubochet J, Fakan S. 2006. Cryoelectron microscopy of vitrified sections: A new challenge for the analysis of functional nuclear architecture. *Histochem Cell Biol* **125:** 43–51.

Branco MR, Pombo A. 2006. Intermingling of chromosome territories in interphase suggests role in translocations and transcription-dependent associations. *PLoS Biol* **4:** e138. doi: 10.1371/journal.pbio.0040138.

Buratowski S. 2009. Progression through the RNA polymerase II CTD cycle. *Mol Cell* **36:** 541–546.

Chapman RD, Heidemann M, Albert TK, Mailhammer R, Flatley A, Meisterernst M, Kremmer E, Eick D. 2007. Transcribing RNA polymerase II is phosphorylated at CTD residue serine-7. *Science* **318:** 1780–1782.

Cook PR. 2010. A model for all genomes: The role of transcription

factories. *J Mol Biol* **395:** 1–10.
Cremer T, Cremer C. 2001. Chromosome territories, nuclear architecture and gene regulation in mammalian cells. *Nat Rev Genet* **2:** 292–301.
Cremer T, Cremer M. 2010. Chromosome territories. *Cold Spring Harb Perspect Biol.* **2:** a003889. doi: 10.1101/cshperspect.a003889.
Cremer C, Edelmann P, Bornfleth H, Kreth G, Muench H, Luz H, Hausmann M. 1999. Principles of spectral precision distance confocal microscopy for the analysis of molecular nuclear structure. In *Handbook of computer vision and applications* (ed. H. Jähne, P Geißler), pp. 839–857. Academic Press, San Diego.
Cremer T, Kreth G, Koester H, Fink RH, Heintzmann R, Cremer M, Solovei I, Zink D, Cremer C. 2000. Chromosome territories, interchromatin domain compartment, and nuclear matrix: An integrated view of the functional nuclear architecture. *Crit Rev Eukar Gene* **10:** 179–212.
Cremer T, Cremer M, Dietzel S, Muller S, Solovei I, Fakan S. 2006. Chromosome territories: A functional nuclear landscape. *Curr Opin Cell Biol* **18:** 307–316.
Cremer C, von Ketteler A, Lemmer P, Kaufmann R, Weiland Y, Mueller P, Hausmann M, Baddeley D, Amberger A. 2010. Far field fluorescence microscopy of cellular structures at molecular resolution. In *Nanoscopy and multidimensional optical fluorescence microscopy* (ed. T Francis), pp. 3-1 to 3-35. CRC Press/Taylor and Francis Group, Boca Raton, FL.
de Gennes PG. 1979. *Scaling concepts in polymer physics*. Cornell University Press, Ithaca, NY.
Dekker J, Rippe K, Dekker M, Kleckner N. 2002. Capturing chromosome conformation. *Science* **295:** 1306–1311.
de Laat W, Grosveld F. 2007. Inter-chromosomal gene regulation in the mammalian cell nucleus. *Curr Opin Genet Dev* **17:** 456–464.
Egloff S, Murphy S. 2008. Cracking the RNA polymerase II CTD code. *Trends Genet* **24:** 280–288.
Eltsov M, Maclellan KM, Maeshima K, Frangakis AS, Dubochet J. 2008. Analysis of cryo-electron microscopy images does not support the existence of 30-nm chromatin fibers in mitotic chromosomes in situ. *Proc Natl Acad Sci* **105:** 19732–19737.
Eskiw CH, Rapp A, Carter DR, Cook PR. 2008. RNA polymerase II activity is located on the surface of protein-rich transcription factories. *J Cell Sci* **121:** 1999–2007.
Fakan S. 2004. Ultrastructural cytochemical analyses of nuclear functional architecture. *Eur J Histochem* **48:** 5–14.
Fakan S, Hancock R. 1974. Localization of newly-synthesized DNA in a mammalian cell as visualized by high resolution autoradiography. *Exp Cell Res* **83:** 95–102.
Fakan S, van Driel R. 2007. The perichromatin region: A functional compartment in the nucleus that determines large-scale chromatin folding. *Semin Cell Dev Biol* **18:** 676–681.
Faro-Trindade I, Cook PR. 2006. A conserved organization of transcription during embryonic stem cell differentiation and in cells with high C value. *Mol Biol Cell* **17:** 2910–2920.
Finan JD, Guilak F. 2010. The effects of osmotic stress on the structure and function of the cell nucleus. *J Cell Biochem* **109:** 460–467.
Gorisch SM, Richter K, Scheuermann MO, Herrmann H, Lichter P. 2003. Diffusion-limited compartmentalization of mammalian cell nuclei assessed by microinjected macromolecules. *Exp Cell Res* **289:** 282–294.
Gorisch SM, Lichter P, Rippe K. 2005. Mobility of multi-subunit complexes in the nucleus: Accessibility and dynamics of chromatin subcompartments. *Histochem Cell Biol* **123:** 217–228.
Grünwald D, Singer RH. 2010. In vivo imaging of labelled endogenous β actin mRNA during nucleocytoplasmic transport. *Nature* **467:** 604–607.
Gunkel M, Erdel F, Rippe K, Lemmer P, Kaufmann R, Hormann C, Amberger R, Cremer C. 2009. Dual color localization microscopy of cellular nanostructures. *Biotechnol J* **4:** 927–938.
Gustafsson MG. 2000. Surpassing the lateral resolution limit by a factor of two using structured illumination microscopy. *J Microsc* **198:** 82–87.
Gustafsson MG, Shao L, Carlton PM, Wang CJ, Golubovskaya IN, Cande WZ, Agard DA, Sedat JW. 2008. Three-dimensional resolution doubling in wide-field fluorescence microscopy by structured illumination. *Biophys J* **94:** 4957–4970.
Haeusler RA, Engelke DR. 2006. Spatial organization of transcription by RNA polymerase III. *Nucleic Acids Res* **34:** 4826–4836.
Heintzmann R, Cremer C. 1999. Laterally modulated excitation microscopy: Improvement of resolution by using a diffraction grating. *Proc SPIE* **3568:** 185–196.
Hell SW. 2009. Microscopy and its focal switch. *Nat Methods* **6:** 24–32.
Hozák P, Jackson DA, Cook PR. 1994. Replication factories and nuclear bodies: The ultrastructural characterization of replication sites during the cell cycle. *J Cell Sci* **107:** 2191–2202.
Huang B, Bates M, Zhuang X. 2009. Super-resolution fluorescence microscopy. *Annu Rev Biochem* **78:** 993–1016.
Hubert J, Bourgeois CA. 1986. The nuclear skeleton and the spatial arrangement of chromosomes in the interphase nucleus of vertebrate somatic cells. *Hum Genet* **74:** 1–15.
Hughes TA, Pombo A, McManus J, Hozák P, Jackson DA, Cook PR. 1995. On the structure of replication and transcription factories. *J Cell Sci Suppl* **19:** 59–65.
Jackson DA, Pombo A. 1998. Replicon clusters are stable units of chromosome structure: Evidence that nuclear organization contributes to the efficient activation and propagation of S phase in human cells. *J Cell Biol.* **140:** 1285–1295.
Jackson DA, Iborra FJ, Manders EM, Cook PR. 1998. Numbers and organization of RNA polymerases, nascent transcripts, and transcription units in HeLa nuclei. *Mol Biol Cell* **9:** 1523–1536.
Jacob F. 1977. Evolution and tinkering. *Science* **196:** 1161–1166.
Jähne B. 2005. *Digitale Bildverarbeitung*, 6th ed. Springer, Heidelberg, Germany.
Jaunin F, Fakan S. 2002. DNA replication and nuclear architecture. *J Cell Biochem* **85:** 1–9.
Jaunin F, Visser AE, Cmarko D, Aten JA, Fakan S. 2000. Fine structural in situ analysis of nascent DNA movement following DNA replication. *Exp Cell Res* **260:** 313–323.
Kim TH, Ren B. 2006. Genome-wide analysis of protein–DNA interactions. *Annu Rev Genomics Hum Genet* **7:** 81–102.
Kimura H, Sugaya K, Cook PR. 2002. The transcription cycle of RNA polymerase II in living cells. *J Cell Biol* **159:** 777–782.
Kind J, van Steensel B. 2010. Genome–nuclear lamina interactions and gene regulation. *Curr Opin Cell Biol* **22:** 320–325.
Koberna K, Ligasova A, Malinsky J, Pliss A, Siegel AJ, Cvackova Z, Fidlerova H, Masata M, Fialova M, Raska I, et al. 2005. Electron microscopy of DNA replication in 3-D: Evidence for similar-sized replication foci throughout S-phase. *J Cell Biochem* **94:** 126–138.
Koehler K, Zakhartchenko V, Froenicke L, Stone G, Stanyon R, Wolf E, Cremer T, Brero A. 2009. Changes of higher order chromatin arrangements during major genome activation in bovine preimplantation embryos. *Exp Cell Res* **315:** 2053–2063.
Kontermann E, Liu Z, Schulze A, Sommer A, Queitsch I, Dubel S, Kipriyano M, Breitling F, Bautz K. 1995. Characterization of the epitope recognized by a monoclonal antibody directed against the largest subunit of *Drosophila* RNA polymerase II. *Biol Chem Hoppe Seyler* **376:** 473–481.
Kreth G, Finsterle J, Cremer C. 2004a. Virtual radiation biophysics: Implications of nuclear structure. *Cytogenet Genome Res* **104:** 157–161.
Kreth G, Finsterle J, von Hase J, Cremer M, Cremer C. 2004b. Radial arrangement of chromosome territories in human cell nuclei: A computer model approach based on gene density indicates a probabilistic global positioning code. *Biophys J* **86:** 2803–2812.
Kreth G, Pazhanisamy SK, Hausmann M, Cremer C. 2007. Cell type-specific quantitative predictions of radiation-induced chromosome aberrations: A computer model approach. *Radiat Res* **167:** 515–525.
Lemmer P, Gunkel M, Weiland Y, Muller P, Baddeley D, Kaufmann R, Urich A, Eipel H, Amberger R, Hausmann M, Cremer C. 2009. Using conventional fluorescent markers for far-field fluorescence localization nanoscopy allows resolution in the 10-nm range. *J Microsc* **235:** 163–171.

Li Q, Barkess G, Qian H. 2006. Chromatin looping and the probability of transcription. *Trends Genet* **22:** 197–202.

Lieberman-Aiden E, van Berkum NL, Williams L, Imakaev M, Ragoczy T, Telling A, Amit I, Lajoie BR, Sabo PJ, Dorschner MO, et al. 2009. Comprehensive mapping of long-range interactions reveals folding principles of the human genome. *Science* **326:** 289–293.

Linnemann AK, Platts AE, Krawetz SA. 2009. Differential nuclear scaffold/matrix attachment marks expressed genes. *Hum Mol Genet* **18:** 645–654.

Lowy DR, Rands E, Scolnick EM. 1978. Helper-independent transformation by unintegrated Harvey sarcoma virus DNA. *J Virol* **26:** 291–298.

Ma H, Samarabandu J, Devdhar RS, Acharya R, Cheng PC, Meng C, Berezney R. 1998. Spatial and temporal dynamics of DNA replication sites in mammalian cells. *J Cell Biol* **143:** 1415–1425.

Maeshima K, Eltsov M. 2008. Packaging the genome: The structure of mitotic chromosomes. *J Biochem* **143:** 145–153.

Maeshima K, Hihara S, Eltsov M. 2010. Chromatin structure: Does the 30-nm fibre exist in vivo? *Curr Opin Cell Biol* **22:** 291–297.

Malyavantham KS, Bhattacharya S, Alonso WD, Acharya R, Berezney R. 2008a. Spatio-temporal dynamics of replication and transcription sites in the mammalian cell nucleus. *Chromosoma* **117:** 553–567.

Malyavantham KS, Bhattacharya S, Barbeitos M, Mukherjee L, Xu J, Fackelmayer FO, Berezney R. 2008b. Identifying functional neighborhoods within the cell nucleus: Proximity analysis of early S-phase replicating chromatin domains to sites of transcription, RNA polymerase II, HP1γ, matrin 3 and SAF-A. *J Cell Biochem* **105:** 391–403.

Martin S, Failla AV, Spori U, Cremer C, Pombo A. 2004. Measuring the size of biological nanostructures with spatially modulated illumination microscopy. *Mol Biol Cell* **15:** 2449–2455.

Mehta IS, Amira M, Harvey AJ, Bridger JM. 2010. Rapid chromosome territory relocation by nuclear motor activity in response to serum removal in primary human fibroblasts. *Genome Biol* **11:** R5. doi: 10.1186/gb-2010-11-1-r5.

Monneron A, Bernhard W. 1969. Fine structural organization of the interphase nucleus in some mammalian cells. *J. Ultrastruct Res* **27:** 266–288.

Münkel C, Eils R, Dietzel S, Zink D, Mehring C, Wedemann G, Cremer T, Langowski J. 1999. Compartmentalization of interphase chromosomes observed in simulation and experiment. *J Mol Biol* **285:** 1053–1065.

Németh A, Conesa A, Santoyo-Lopez J, Medina I, Montaner D, Péterfia B, Solovei I, Cremer T, Dopazo J, Längst G. 2010. Initial genomics of the human nucleolus. *PLoS Genet* **6:** e1000889. doi: 10.1371/journal.pgen.1000889.

Nickerson JA, Krockmalnic G, Wan KM, Penman S. 1997. The nuclear matrix revealed by eluting chromatin from a cross-linked nucleus. *Proc Natl Acad Sci* **94:** 4446–4450.

Niedojadlo J, Perret-Vivancos C, Kalland K-H, Cmarko D, Cremer C, van Driel R, Fakan S. 2011. Transcribed DNA is preferentially located in the perichromatin region of mammalian cell nuclei. *Exp Cell Res* **317:** 433–444.

Osborne CS, Chakalova L, Mitchell JA, Horton A, Wood AL, Bolland DJ, Corcoran AE, Fraser P. 2007. *Myc* dynamically and preferentially relocates to a transcription factory occupied by *Igh*. *PLoS Biol* **5:** e192. doi: 10.1371/journal.pbio.0050192.

Palstra RJ, Simonis M, Klous P, Brasset E, Eijkelkamp B, de Laat W. 2008. Maintenance of long-range DNA interactions after inhibition of ongoing RNA polymerase II transcription. *PLoS One* **3:** e1661. doi: 10.1371/journal.pone.0001661.

Patterson G, Davidson M, Manley S, Lippincott-Schwartz J. 2010. Superresolution imaging using single-molecule localization. *Annu Rev Phys Chem* **61:** 345–367.

Philimonenko AA, Hodný Z, Jackson DA, Hozák P. 2006. The microarchitecture of DNA replication domains. *Histochem Cell Biol* **125:** 103–117.

Postberg J, Alexandrova O, Cremer T, Lipps HJ. 2005. Exploiting nuclear duality of ciliates to analyse topological requirements for DNA replication and transcription. *J Cell Sci* **118:** 3973–3983.

Postberg J, Heyse K, Cremer M, Cremer T, Lipps HJ. 2008. Spatial and temporal plasticity of chromatin during programmed DNA-reorganization in *Stylonychia* macronuclear development. *Epigenetics Chromatin* **1:** 3. doi: 10.1186/1756-8935-1-3.

Postberg J, Lipps HJ, Cremer T. 2010. Evolutionary origin of the cell nucleus and its functional architecture. *Essays Biochem* **48:** 1–24.

Reymann J, Baddeley D, Gunkel M, Lemmer P, Stadter W, Jegou T, Rippe K, Cremer C, Birk U. 2008. High-precision structural analysis of subnuclear complexes in fixed and live cells via spatially modulated illumination (SMI) microscopy. *Chromosome Res* **16:** 367–382.

Rouquette J, Genoud C, Vazquez-Nin GH, Kraus B, Cremer T, Fakan S. 2009. Revealing the high-resolution three-dimensional network of chromatin and interchromatin space: A novel electron-microscopic approach to reconstructing nuclear architecture. *Chromosome Res* **17:** 801–810.

Rouquette J, Cremer C, Cremer T, Fakan S. 2010. Functional nuclear architecture studied by microscopy: Present and future. *Int Rev Cell Mol Biol* **282:** 1–90.

Rust MJ, Bates M, Zhuang X. 2006. Sub-diffraction-limit imaging by stochastic optical reconstruction microscopy (STORM). *Nat Methods* **3:** 793–795.

Schermelleh L, Solovei I, Zink D, Cremer T. 2001. Two-color fluorescence labeling of early and mid-to-late replicating chromatin in living cells. *Chromosome Res* **9:** 77–80.

Schermelleh L, Carlton PM, Haase S, Shao L, Winoto L, Kner P, Burke B, Cardoso MC, Agard DA, Gustafsson MG, et al. 2008. Subdiffraction multicolor imaging of the nuclear periphery with 3D structured illumination microscopy. *Science* **320:** 1332–1336.

Schermelleh L, Heintzmann R, Leonhardt H. 2010. A guide to super-resolution fluorescence microscopy. *J Cell Biol* **190:** 165–175.

Schoenfelder S, Sexton T, Chakalova L, Cope NF, Horton A, Andrews S, Kurukuti S, Mitchell JA, Umlauf D, Dimitrova DS, et al. 2010. Preferential associations between co-regulated genes reveal a transcriptional interactome in erythroid cells. *Nat Genet* **42:** 53–61.

Sinclair P, Bian Q, Plutz M, Heard E, Belmont AS. 2010. Dynamic plasticity of large-scale chromatin structure revealed by self-assembly of engineered chromosome regions. *J Cell Biol* **190:** 761–776.

Solimando L, Luijsterburg MS, Vecchio L, Vermeulen W, van Driel R, Fakan S. 2009. Spatial organization of nucleotide excision repair proteins after UV-induced DNA damage in the human cell nucleus. *J Cell Sci* **122:** 83–91.

Solovei I, Kreysing M, Lanctot C, Kosem S, Peichl L, Cremer T, Guck J, Joffe B. 2009. Nuclear architecture of rod photoreceptor cells adapts to vision in mammalian evolution. *Cell* **137:** 356–368.

Sparvoli E, Levi M, Rossi E. 1994. Replicon clusters may form structurally stable complexes of chromatin and chromosomes. *J Cell Sci* **107:** 3097–3103.

Steiner LA, Maksimova Y, Schulz V, Wong C, Raha D, Mahajan C, Weissman M, Gallagher G. 2009. Chromatin architecture and transcription factor binding regulate expression of erythrocyte membrane protein genes. *Mol Cell Biol* **29:** 5399–5412.

Strickfaden H, Zunhammer A, van Koningsbruggen S, Kohler D, Cremer T. 2010. 4D chromatin dynamics in cycling cells: Theodor Boveri's hypotheses revisited. *Nucleus* **1:** 1–14.

Strickfaden H, Cremer T, Rippe K. 2011. Higher order chromatin organization and dynamics. In *Genome organization and function in the mammalian cell nucleus* (ed. K Rippe). Wiley-VCH, Weinheim.

Tashiro S, Muto A, Tanimoto K, Tsuchiya H, Suzuki H, Hoshino H, Yoshida M, Walter J, Igarashi K. 2004. Repression of PML nuclear body-associated transcription by oxidative stress-activated Bach2. *Mol Cell Biol* **24:** 3473–3484.

Trumtel S, Léger-Silvestre I, Gleizes PE, Teulières F, Gas N. 2000. Assembly and functional organization of the nucleolus: Ultrastructural analysis of *Saccharomyces cerevisiae* mutants. *Mol Biol Cell* **11:** 2175–2189.

Van Steensel B, Henikoff S. 2000. Identification of in vivo DNA targets of chromatin proteins using tethered dam methyltransferase. *Nat Biotechnol* **18:** 424–428.

von Schack ML, Fakan S, Villiger W, Müller M. 1993. Cryofixation and cryosubstitution: A useful alternative in the analyses of cellular fine structure. *Eur J Histochem* **37:** 5–18.

Wang P, Lin C, Smith ER, Guo H, Sanderson BW, Wu M, Gogol M, Alexander T, Seidel C, Wiedemann LM, et al. 2009. Global analysis of H3K4 methylation defines MLL family member targets and points to a role for MLL1-mediated H3K4 methylation in the regulation of transcriptional initiation by RNA polymerase II. *Mol Cell Biol* **29:** 6074–6085.

Wei X, Samarabandu J, Devdhar RS, Siegel AJ, Acharya R, Berezney R. 1998. Segregation of transcription and replication sites into higher order domains. *Science* **281:** 1502–1506.

Wiedemann SM, Mildner SN, Bönisch C, Israel L, Maiser A, Matheisl S, Straub T, Merkl R, Leonhardt H, Kremmer E, et al. 2010. Identification and characterization of two novel primate-specific histone H3 variants, H3.X and H3.Y. *J Cell Biol* **190:** 777–791.

Zink D, Bornfleth H, Visser A, Cremer C, Cremer T. 1999. Organization of early and late replicating DNA in human chromosome territories. *Exp Cell Res* **247:** 176–188.

Zinner R, Albiez H, Walter J, Peters AH, Cremer T, Cremer M. 2006. Histone lysine methylation patterns in human cell types are arranged in distinct three-dimensional nuclear zones. *Histochem Cell Biol* **125:** 3–19.